frontiers | Frontiers in Earth Science

TYPE Original Research
PUBLISHED 26 March 2025
DOI 10.3389/feart.2025.1552125

OPEN ACCESS

EDITED BY
Jiangyu Wu,
China University of Mining and Technology, China

REVIEWED BY
Yubin Bai,
Xi'an Shiyou University, China
Xiang Wang,
Institute of Geographic Sciences and Natural Resources Research, Chinese Academy of Sciences (CAS), China

*CORRESPONDENCE
Chunjuan Zang,
zangchunjuan_929@163.com

RECEIVED 27 December 2024
ACCEPTED 14 March 2025
PUBLISHED 26 March 2025

CITATION
Gong W, Zang C, Ma J, Sun Y, Zhang H, Xu P and Jiang M (2025) Hydrochemical characteristics and controlling factors of deep karst groundwater in Huaibei Plain, Huaihe River Basin, China.
Front. Earth Sci. 13:1552125.
doi: 10.3389/feart.2025.1552125

Hydrochemical characteristics and controlling factors of deep karst groundwater in Huaibei Plain, Huaihe River Basin, China

Wei Gong[1,2], Chunjuan Zang[1,2]*, Jie Ma[1,2], Yonggang Sun[1,2], Haitao Zhang[1,2], Pan Xu[1,2] and Mingming Jiang[1,2]

[1]School of Resources and Civil Engineering, Suzhou University, Suzhou, China, [2]National Engineering Research Center of Coal Mine Water Hazard Controlling, Suzhou, China

Introduction: Deep karst groundwater is an important object for groundwater resources development and utilisation in the context of increasing water scarcity, as well as a potential threat of water hazards to the deep mining of hidden coalfields in Huaihe River Basin.

Methods: To elucidate the hydrochemical characteristics and controlling factors of deep karst groundwater, groundwater samples in Huaibei Plain were collected and discussed by comprehensively using mathematical statistics, the Piper trilinear diagram, Gibbs diagram, hydrogen and oxygen isotopes, saturation index, ion ratio relationship, and APCS-MLR receptor model.

Results: The absolute principal component score (APCS) with eigenvalues greater than 1 was extracted, where APCS1 could be defined as evaporite minerals and APCS2 could be defined as silicate minerals with a cumulative contribution of 88.63%. The linear fitting results showed that the R^2 values of were above 0.75 with the maximum value reaching 0.92, and the ratios of the measured values to the predicted values were generally close to 1, indicating that the analysis of the APCS-MLR receptor model were credible.

Discussion: The hydrochemical components of deep karst groundwater mainly came from three sources, including evaporite minerals, silicate minerals and unknown sources, and the contributions to the deep groundwater were 59.57%, 29.06% and 11.37%, respectively. The weathering and dissolution of evaporite minerals and silicate minerals were the main sources of the hydrochemical components, and also the main controlling factors for the hydrochemical evolution of deep karst groundwater in Huaihe River Basin.

KEYWORDS

hydrochemical characteristics, hydrogen and oxygen isotopes, saturation index, APCS-MLR, Huaihe river basin

Highlights

- Deep karst groundwater is mainly recharged by atmospheric precipitation, and water-rock interaction constantly occur during karst groundwater

runoff, which in turn controls the hydrochemical evolution.
- Evaporite minerals and silicate minerals are mainly dissolved, and carbonate minerals are precipitated.
- The hydrochemical composition of karst groundwater mainly comes from evaporite minerals, silicate minerals and unknown sources, which contribute 59.57%, 29.06% and 11.37%, respectively.

1 Introduction

As a scarce resource indispensable to all economic life, the use and security of water resources have always been of great concern to developing countries and emerging economies. The intensification of human activities, particularly as a result of the development of the mining industry and related industries, has caused a series of karst water environmental problems, such as the decline of the regional groundwater level, and the continuous and irreversible deterioration of water quality. As the largest hidden coalfield in East China, the Huaibei coalfield in the Huaibei Plain of Huaihe River Basin has experienced more than 60 years of extraction and production, and with the increase of mining depth, the confinement of the deep aquifer is destroyed and the alternation rate of groundwater increases, thus affecting the degree of water-rock interaction (Ju et al., 2022; Chen et al., 2023; Wu et al., 2024). Therefore, it is of great significance to carry out research on the deep aquifer system to grasp the hydrochemical characteristics and controlling factors of karst groundwater for the protection and utilisation of deep water resources.

The hydrochemical characteristics of groundwater is closely related to the geochemical evolution and cycling processes it undergoes, and the spatial distribution and temporal changes are important indicators of the generation, storage (adsorption) and production of resources such as oil and coal bed methane (CBM) (Rizzo et al., 2020; Lu et al., 2022; Warrack et al., 2022; Abdrashitova and Kadyrov 2022). Currently, conventional hydrochemistry, trace element hydrochemistry and isotope hydrochemistry are widely and integrally applied to the hydrogeochemical study of groundwater, of which conventional hydrochemistry mainly focuses on the evaluation of water quality, identification of pollution source, classification of hydrochemical types, water-rock interactions, simulation of hydrochemical processes, and hydrochemical evolution (Li et al., 2021; Jiang et al., 2023; Mehana et al., 2022; Wang et al., 2022), while trace element hydrochemistry mainly focuses on exploration of the recharge-discharge relationship between different water sources, groundwater runoff traceability and the influencing factors of rare earth elements (Poletaeva et al., 2022; Sun et al., 2023; Tran et al., 2023), and isotope hydrochemistry focuses on the determination of groundwater age, the indication of groundwater sources and evaluation of groundwater movement mechanism (Chen et al., 2020; Pan et al., 2023).

The identification of hydrochemistry sources and pollution sources has gradually become a hot spot in current hydrochemistry research, and methods such as isotope tracing, factor analysis (FA), principal component analysis (PCA), PMF receptor model, and APCS-MLR receptor model have been widely used (Abdelaziz et al., 2020; Fatima et al., 2022; Athauda et al., 2023; Mu et al., 2023). Factor analysis (FA) and principal component analysis (PCA) illustrate the main information extracted from multivariate variables by analyzing the interrelationships among the observed indicators with a small number of representative main factors, but it is difficult to achieve a quantitative description of the degree of influence of the principal factors on the observation of a single indicator with PCA or FA alone (Mahanty et al., 2023), and The APCS-MLR receptor model is an optimisation of PCA, where the absolute principal component score (APCS) of each indicator is obtained by subtracting the factor scores that are absolutely zero, and the contribution of APCS to each water body indicator is calculated separately using the APCS as the independent variable and the raw data as the dependent variable (Varol et al., 2022; Li et al., 2023).

Currently, methods such as cluster analysis, fuzzy mathematical evaluation, principal component analysis (PCA), and isotope tracing have been applied to the hydrochemical characteristics and evolution of deep karst groundwater in the Huaihe River Basin (Liu et al., 2020; Chen et al., 2022; Wang et al., 2022), and there is a lack of quantitative studies on the controlling factors of deep karst groundwater and genesis identification, which leads to the inability to determine the impact extent of different water-rock interactions (Zhang et al., 2022; Qiu et al., 2023). Therefore, considering that the impact of industrial and agricultural activities on deep groundwater tends to be small compared to surface water and shallow groundwater, this study adopts the APCS-MLR receptor model for genesis identification to determine the contribution of different water-rock actions to the hydrochemical composition. In addition, a comparative analysis of model fits will be performed to reveal the applicability of the APCS-MLR receptor model in analyzing deep groundwater genesis.

In this study, we studied the hydrochemical characteristics of deep karst groundwater, and analyzed the controlling factors of hydrochemical composition. Multiple methods of mathematical statistics, graphical methods, saturation index, and ion ratio were used. The main objectives of the study were: (1) to clarify the hydrochemical characterization, (2) to perform the sources identification of deep groundwater, (3) to determine the contribution of different water-rock actions to hydrochemical composition. This study provides a scientific basis for the rational development and use of deep water resources in Huaibei Plain of Huaihe River Basin.

2 Materials and methods

2.1 General overview of the study area

As one of the nine major river basins in China, the Huaihe River Basin, with the geographical coordinates of E111°55′- E121°20′, N30°55′- N36°20′, covers an area of 270,000 km^2, with a total population of 165 million people and an arable land area of 13.33 million hm^2. It is one of the regions with the highest population density and arable land rate of all river basins in China, and also one of the regions with the lowest *per capita* water resources possession in China. In 2012, the total water resources of the basin were 64.76 billion m^3, of which 18.15 billion m^3 was underground water resources, and in 2022, the total water resources of the basin were 58.28 billion m^3, of which 30.36 billion m^3 was underground water resources, and the share of the

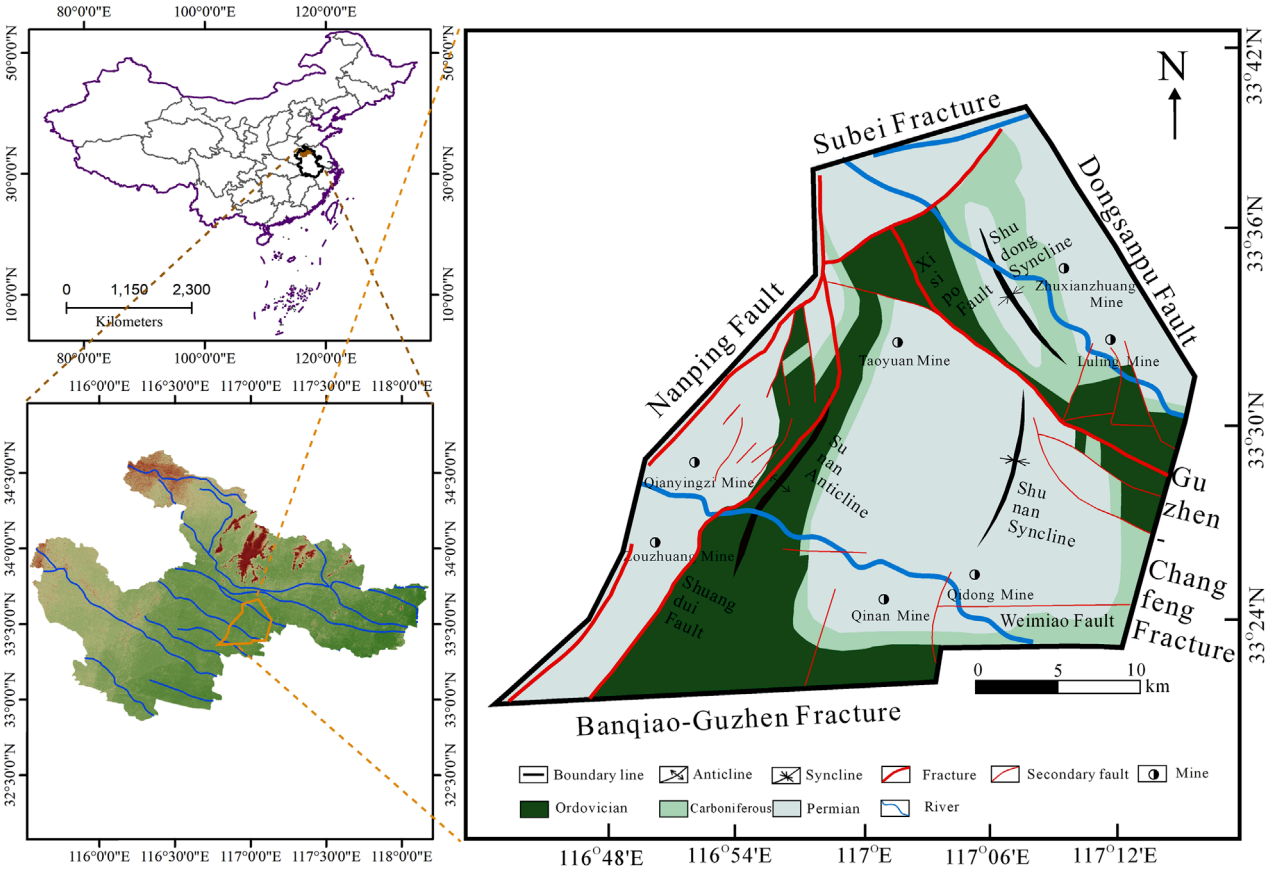

FIGURE 1
Hydrogeological map of the study area.

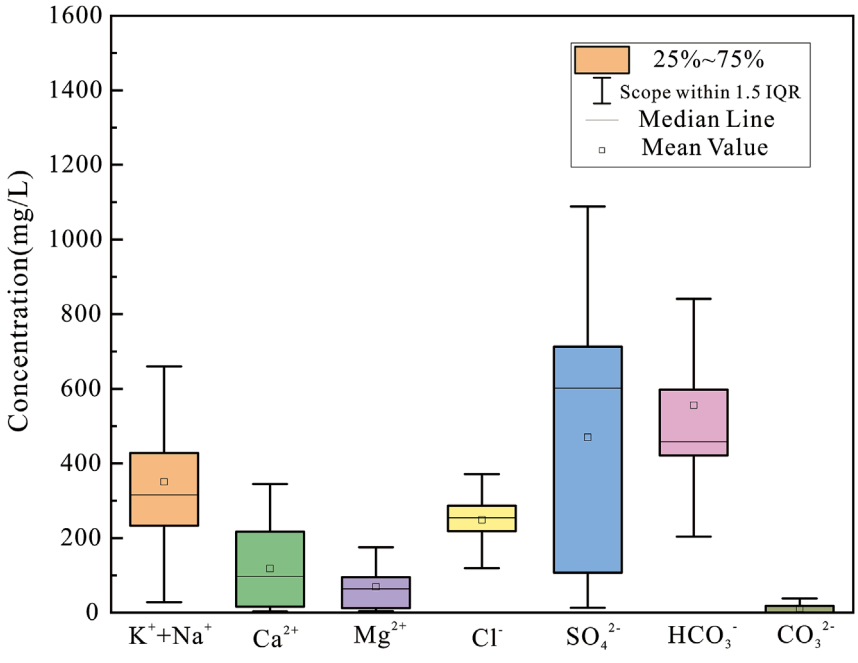

FIGURE 2
Box plot of major ion content.

TABLE 1 Characteristics of hydrochemical components of deep karst groundwater (mg/L).

Index	K^++Na^+	Ca^{2+}	Mg^{2+}	Cl^-	SO_4^{2-}	HCO_3^-	CO_3^{2-}	TDS	pH
Maximum value	809.19	344.69	175.32	658.72	1,088.27	1,320.38	167.05	2,474.50	8.7
Minimum value	28.02	3.70	4.09	68.03	13.17	204.15	0.00	577.21	6.9
Mean value	347.42	114.50	56.60	241.59	454.15	549.92	13.09	1,502.30	7.8
Standard deviation	160.01	100.86	42.79	85.80	332.55	235.21	26.25	441.49	0.54
Variation coefficient	0.46	0.88	0.76	0.36	0.73	0.43	2.01	0.29	0.07

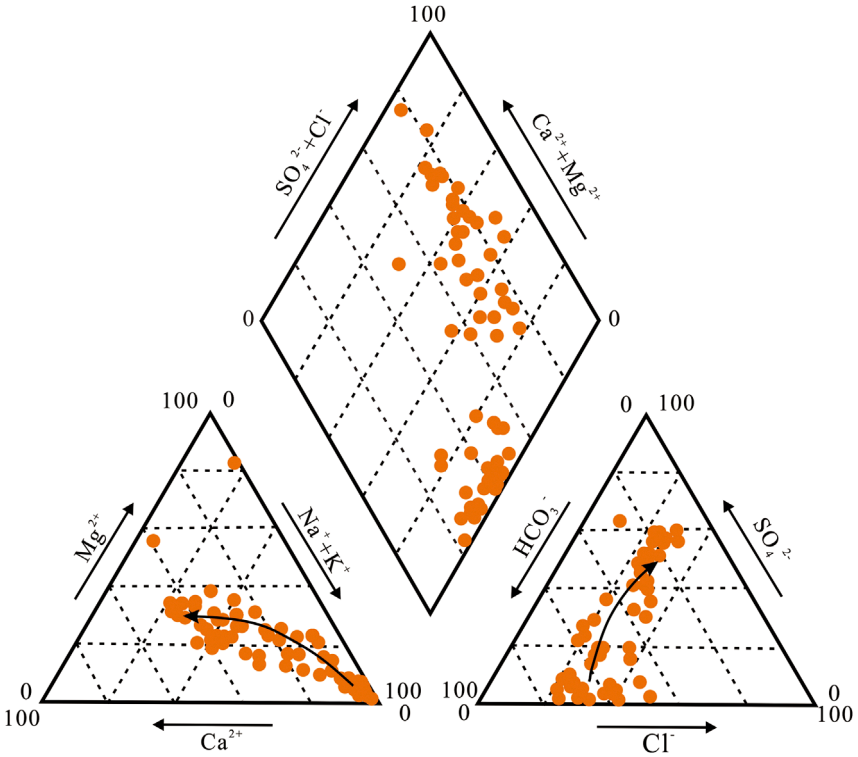

FIGURE 3
Piper trilinear diagram of deep karst groundwater.

water resources increased from 28.0% to 52.1%. In the last decade, groundwater resources have been playing an increasingly important role in the basin for irrigated agriculture, industrial production and domestic water use.

As the main study area, the Sunan mining area of Huaibei Plain is a typical hidden coal mining area and located in the central part of HRB, covering an area of about 1,050 km^2. The topography of the main study area is flat, with ground elevations generally ranging from 23 m to 32 m. The groundwater system is a complex groundwater system composed of several aquifers, and the main aquifers from top to bottom are: Cenozoic Loose Layer Pore Aquifer, Permian Coal System Sandstone Fissure Aquifer, Carboniferous Karst Fissure Aquifer and Ordovician limestone Karst Fissure Aquifer. As the main research object, the water-richness of the Carboniferous Karst Fissure Aquifer is controlled by the degree of karst development, and the karst groundwater is dominated by horizontal runoff, with slow runoff rate (Zhang et al., 2022; Chen et al., 2023; Wu et al., 2025).

As the secondary hydrological unit, the Sunan mining area has a relatively complete and independent groundwater recharge, runoff and discharge system, and the overall direction of limestone groundwater runoff in the region is from southeast to northwest (Figure 1). The seven coal mines in the mining area selected for the study are located in the east, middle and west of the hydrogeological unit, which play a good role in controlling the hydrochemical characteristics and formation mechanism of Carboniferous Karst Fissure Aquifer (Gu et al., 2023). Specifically, the Zhuxianzhuang and Luling mines are located in the northeastern part of the hydrogeologic unit, which is in the southeast to northwest runoff

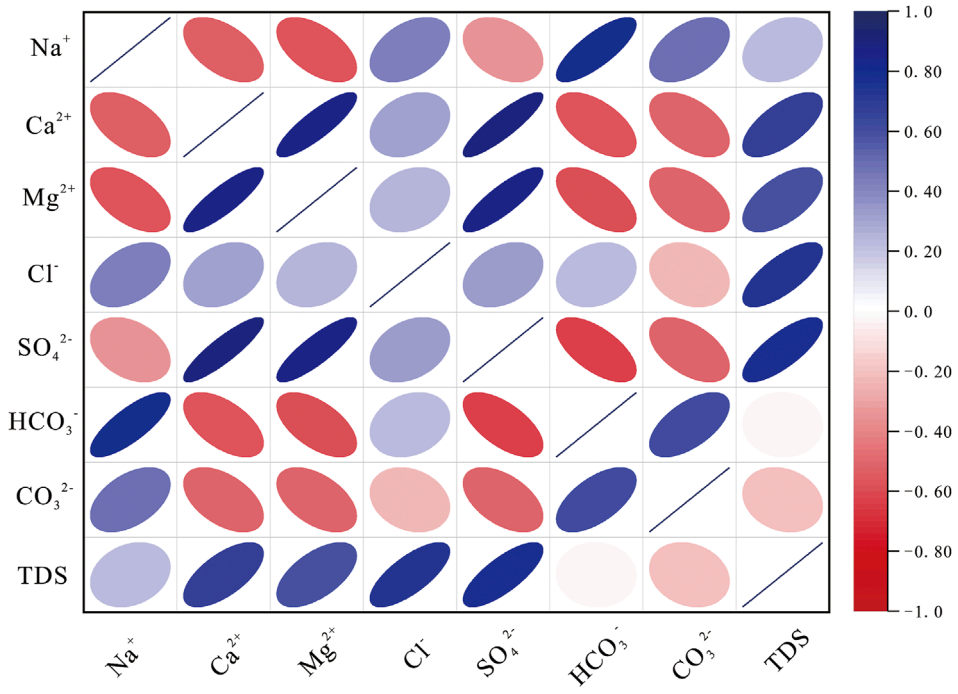

FIGURE 4
Correlation of the hydrochemical components.

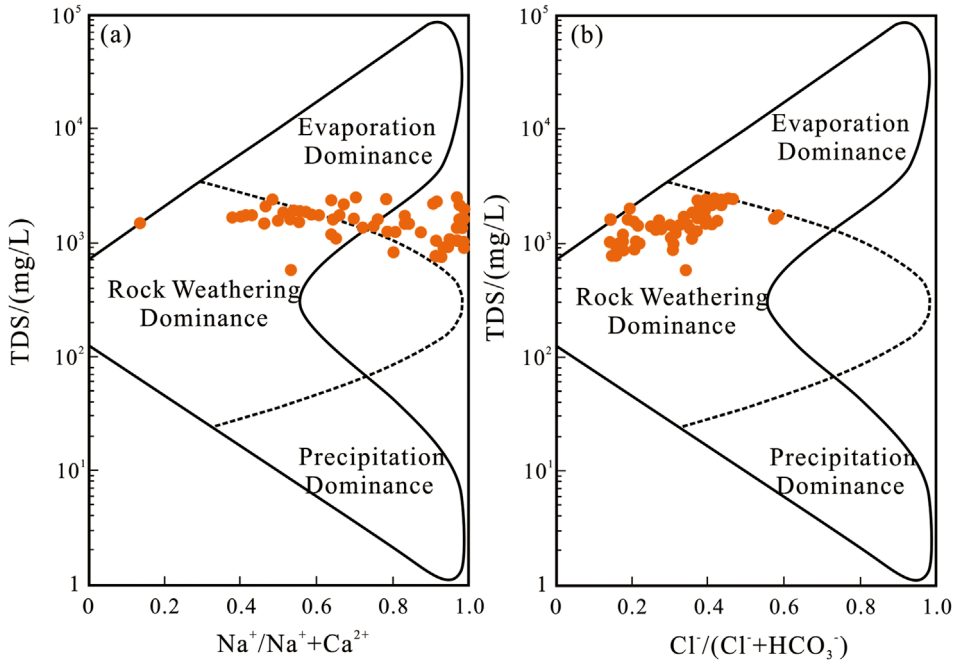

FIGURE 5
Gibbs diagram.

zone of deep karst groundwater; the Qinan, Qidong, and Taoyuan mines are located in the central part, which is in the south to north runoff zone; and the Zouzhuang and Qanyingzi mines are located in the western part, which is in the southwest to northeast runoff zone.

2.2 Sampling and testing

From March 2023 to July 2023, a total of 10 rainwater samples and 75 karst groundwater samples were collected from the target

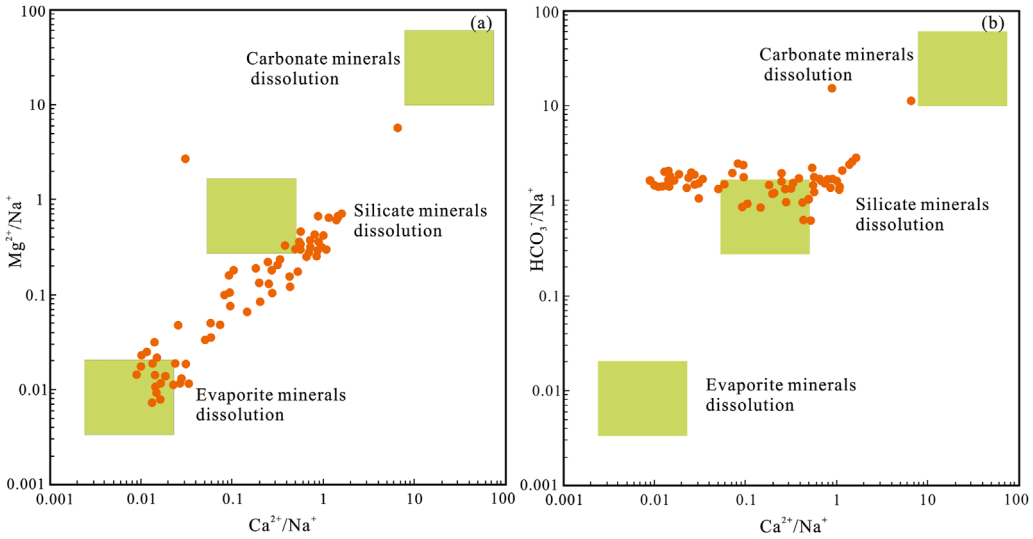

FIGURE 6
Ratio diagram of Ca^{2+}/Na^{+} - Mg^{2+}/Na^{+} and Ca^{2+}/Na^{+} - HCO_3^{-}/Na^{+}.

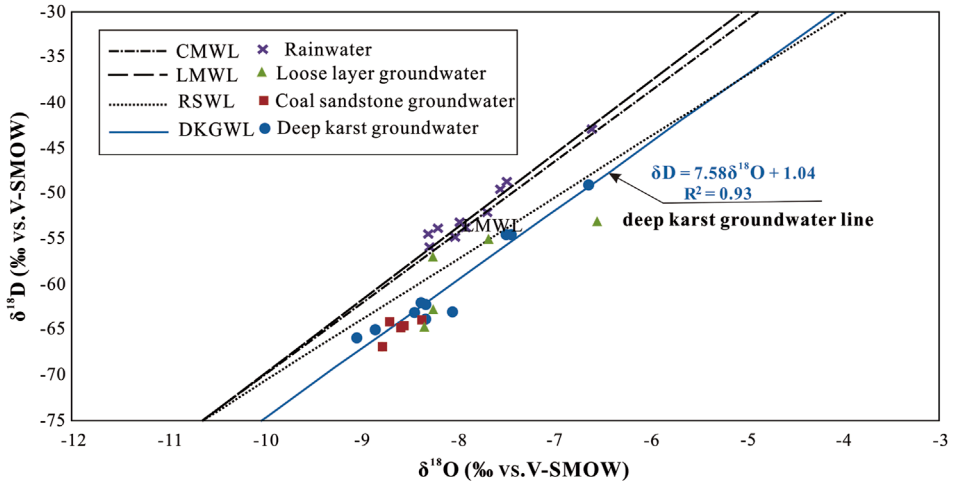

FIGURE 7
Isotopic signature of hydrogen and oxygen in different water bodies.

layer in the study area of the Huaihe River Basin. Each sample was filtered (pore size 0.45 μm) and fixed with acid (HNO_3) at the time of collection, and all samples were stored in sealed polyethylene bottles for cold storage. The pH and TDS of the water samples were determined on site using a portable instrument (OHAUS, Shanghai). The main anion and cation concentrations were done in the laboratory of the National Engineering Research Center of Coal Mine Water Hazard Controlling, where Ca^{2+} and Mg^{2+} were tested with an ion chromatography (ICS - 600), with a testing accuracy of RSD <1%; K^{+}, Na^{+}, Cl^{-} and SO_4^{2-} were tested with an ion chromatography (ICS - 900), with a testing accuracy of RSD <0.1%, HCO_3^{-} was measured by acid-base titration, and the total dissolved solids (TDS) were determined using the drying method. δD and $\delta^{18}O$ were tested using the LGR Liquid Water Isotope Analyzer (912–0026) using the Vienna Mean Ocean Water Standard (V - SMOW) as the reference standard, where δD and $\delta^{18}O$ were analysed with an accuracy of ±0.2‰ and ±0.03‰, respectively.

Considering the existence of subjective and objective errors in the course of testing, the test data were subjected to anion and cation balance test with the test equation, and the E values of the samples were −3.28% ~2.65%, which all met the requirements.

2.3 Data processing

In this study, raw hydrochemical data were collated and counted using Excel 2021, and Piper trilinear plots, Gibbs plots, and ion-concentration-ratio plots were drawn using Origin Pro

TABLE 2 Hydrogen and oxygen isotopes in different water bodies.

Water body	δD			$\delta^{18}O$			d-excess		
	Maximum value/‰	Minimum value/‰	Average value/‰	Maximum value/‰	Minimum value/‰	Average value/‰	Maximum value/‰	Minimum value/‰	Average value/‰
Rainwater (N = 10)	−42.93	−55.90	−51.87	−6.60	−8.33	−7.81	12.37	9.35	10.60
Loose layer groundwater (N = 5)	−53.14	−64.70	−58.60	−6.55	−8.34	−7.81	9.02	−0.76	3.89
Coal sandstone groundwater (N = 5)	−64.00	−66.90	−64.94	−8.36	−8.78	−8.60	5.40	2.88	3.88
Deep karst groundwater (N = 10)	−49.09	−65.95	−60.35	−6.64	−9.04	−8.10	6.34	1.29	4.43

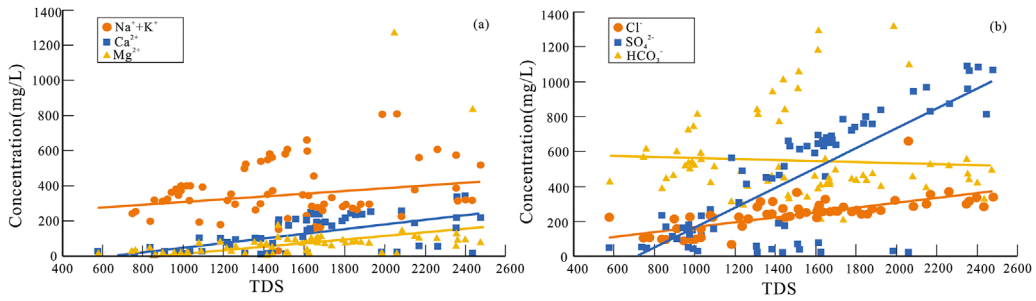

FIGURE 8
Relationship between concentration of major ions and TDS.

to determine the hydrochemical type and ion ratio relationships of karst groundwater, thereby revealing the sources of the ionic components and the controlling factors. The saturation indices of different minerals in karst groundwater were calculated using PHREEQC3.7. Quantitative analysis of the genesis of deep karst groundwater in the study area receptor model was carried out using SPSS21 and the APCS-MLR receptor model to determine the contribution of each genesis source to the hydrochemical indices, and the correctness of the results of the genesis analyses was examined by the linear fit between the predicted and measured concentrations of the regression model.

3 Results and discussion

3.1 Hydrochemical characterization of major ion

According to the results of the hydrochemical tests, the cations of deep karst groundwater were dominated by Na^+ and Ca^{2+}, with concentrations of 28.02–809.19 mg/L and 3.7–344.69 mg/L, respectively, which were characterized by $Na^+ > Ca^{2+} > Mg^{2+}$. The anions were dominated by HCO_3^- and SO_4^{2-}, with concentrations of 204.15–1,320.38 mg/L and 13.17–1,088.27 mg/L, respectively, which were characterized by $HCO_3^- > SO_4^{2-} > Cl^- > CO_3^{2-}$ (Figure 2). The variation of the TDS ranged from 577.21 to 2,474.5 mg/L, and pH varied from 6.9 to 8.7, which was neutral-weakly alkaline water (Table 1). The coefficients of variation (CV) of the major ions in karst groundwater ranged from 0.36 to 2.01, indicating that the distribution of the major ions in the groundwater had a medium-high spatial variability, among which CO_3^{2-} had the highest spatial variability with a CV value of 2.01. The CV of pH was 0.07, indicating that pH in deep karst groundwater were relatively stable with low variability.

3.2 Hydrochemical types

Piper trilinear diagram using the results of hydrochemical tests provide a visual representation of the relative abundance and distribution characteristics of the major ions to identify the hydrochemical types of water body (Meng et al., 2022; Bian et al., 2023). As can be seen from Figure 3, the distribution of hydrochemical types in karst groundwater was relatively

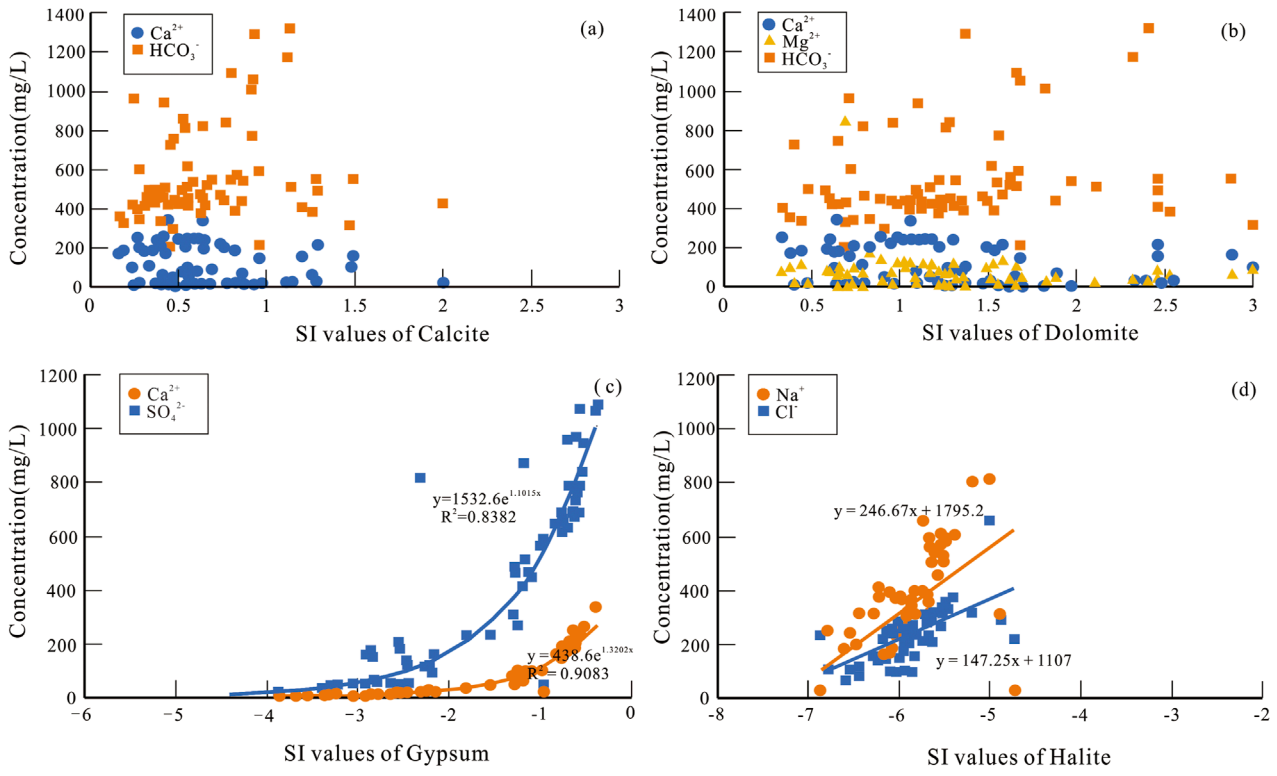

FIGURE 9
Relationship between SI of main minerals and concentrations of major ions.

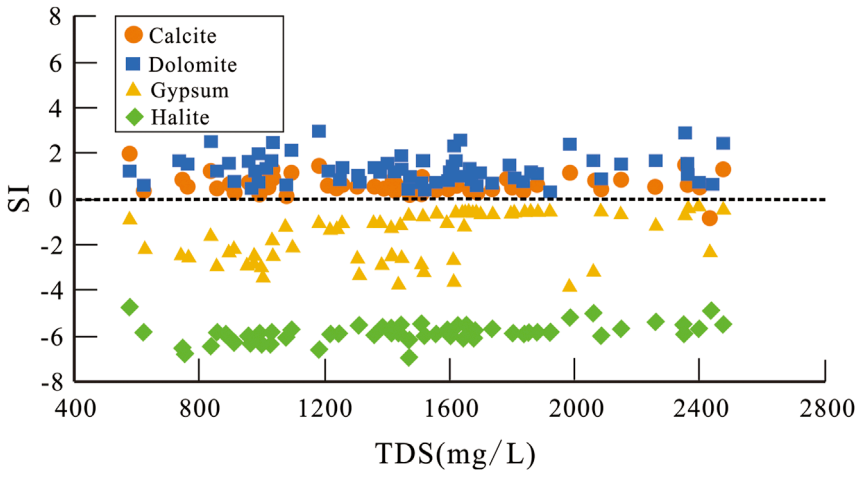

FIGURE 10
Correlation between SI of different minerals and TDS in karst groundwater.

concentrated, with the cations mainly distributed in the Na^+ and Ca^{2+} ends, and the anions mainly distributed in the HCO_3^- and SO_4^{2-} ends, and the hydrochemical types were mainly of the HCO_3 - Na and SO_4 -Na. Ca type. In addition, the hydrochemical components showed a significant change rule along the runoff path, in which the anion dominated by HCO_3^- gradually transitioned to SO_4^{2-} dominated, the cation gradually changed from Ca^{2+} dominated to Na^+ and Ca^{2+} dominated, and the hydrochemical type of groundwater transitioned from the HCO_3 - Na type to the SO_4 - Na. Ca type, which was mainly related to the slow rate of groundwater runoff and the long retention time of karst groundwater in the hydrogeological unit.

TABLE 3 Rotational composition matrix of deep karst groundwater.

Index	APCS1	APCS2
Na+	0.115	0.958
Ca^{2+}	0.888	−0.307
Mg^{2+}	0.91	−0.283
Cl^{-}	0.91	0.159
SO42-	0.983	−0.001
HCO_3^{-}	−0.528	0.696
Eigenvalue	3.278	1.222
Contribution rate/%	59.565	29.061
Cumulative contribution rate/%	59.565	88.626

3.3 Correlation analysis of the hydrochemical components

By analyzing the similarities between the hydrochemical components in groundwater, it can be judged whether the different ions in the hydrochemical components have the same source or similar migration and transformation pathways. The correlation of the hydrochemical components of deep karst groundwater was shown in Figure 4, in which Na^+ and HCO_3^- showed a significant positive correlation ($P < 0.01$) with a correlation coefficient of 0.79, while Na^+ and Cl^- showed a correlation coefficient of 0.43 ($P < 0.01$), suggesting that the migration paths of Na^+ and HCO_3^- were similar and both of them might be originated from the weathering and dissolution of silicate minerals. Ca^{2+} showed significant positive correlations with Mg^{2+} and SO_4^{2-} ($P < 0.01$), with correlation coefficients of 0.86 and 0.88, respectively, suggesting that Ca^{2+}, Mg^{2+} and SO_4^{2-} had the same origin or similar migration, which might all come from the weathering and dissolution of evaporite minerals. TDS showed a significant positive correlation with Ca^{2+}, Mg^{2+}, Cl^-, and SO_4^{2-} ($P < 0.01$), with correlation coefficients of 0.66, 0.6, 0.74, and 0.77, respectively, indicating that Ca^{2+}, Mg^{2+}, Cl^- and SO_4^{2-} contributed relatively more to TDS compared with other ions.

3.4 Analysis of controlling factors

3.4.1 Mechanisms of water-rock interactions

The Gibbs diagram can be used to determine the dominant factors affecting the hydrochemical components of the water body. The Gibbs ratio, i.e., the ratio of $Na^+/(Na^+ + K^+)$ and $Cl^-/(Cl^- + HCO_3^-)$ to TDS, can be used to visually depict the controlling effects of evaporation, rock weathering, precipitation, *etc.*, on the hydrochemistry (Yu et al., 2022). As can be seen from Figure 5, the samples of deep karst groundwater were mainly located between rock weathering dominance area and the evaporation dominance area, and were far away from the precipitation dominance area, which indicated that the water-rock interactions and evaporation action played an important role in the hydrochemical components of deep karst groundwater.

Different types of rock weathering cause ion differences in the water body, and the main types of water-rock interactions can be further determined by the correlation ratios of Ca^{2+}/Na^+ to Mg^{2+}/Na^+ and Ca^{2+}/Na^+ to HCO_3^-/Na^+, among which common types of water-rock interactions are the weathering and dissolution of silicate minerals, evaporite minerals and carbonate minerals. The samples of deep groundwater were located in the dominant zone of silicate minerals and evaporite minerals (Figure 6), indicating that the weathering and dissolution of silicate minerals and the dissolution of evaporite minerals were the main types of water-rock interactions.

3.4.2 Isotopic signature of hydrogen and oxygen

Stable isotope tracing techniques are often used to reveal the cyclic evolutionary processes of surface water and groundwater and the recharge-transformation relationships between different water bodies. Considering the regional variability of the precipitation in different areas, the Local Meteorological Precipitation Line (LMWL) was established with reference to the atmospheric precipitation line of the adjacent Zhengzhou area: $\delta D = 8.07\ \delta^{18}O + 10.75$, $R^2 = 0.97$. Compared with CMWL, the slope of LMWL (8.07) and the intercept (10.75) were both larger than that of CMWL (Figure 7), which indicated that the study area was less affected by local re-circulation of water vapour. The sample points of deep karst groundwater were mainly distributed on the right side of LMWL and Regional Surface Water Line (RSWL), which indicated that the deep karst groundwater mainly came from the recharge of atmospheric precipitation. The slope of the deep karst groundwater line (7.58) was slightly smaller than the slope of CMWL (7.83) and the slope of LMWL (8.07), indicating that in the process of recharging the deep karst groundwater by atmospheric precipitation, the water body was subjected to a certain degree of evaporation, which resulted in the isotopic fractionation of hydrogen and oxygen. Compared with the deep karst groundwater, the δD and $\delta^{18}O$ of the coal sandstone groundwater and loose layer groundwater were relatively positive, indicating that the closer the aquifer was to the surface, the stronger the evaporation of the water body was, and the effect of evaporation fractionation was more significant. The deuterium surplus (d-excess) parameter is a measure of the evaporation degree of the water body recharged to the groundwater, and the more negative the value of d-excess is, the stronger the evaporation effect is. The d-excess values of the deep karst groundwater were all positive, ranging from 1.29‰ to 6.34‰, with a mean value of 4.43‰, which was obviously deviating from the average value of the local atmospheric precipitation (10.75‰), whereas the deuterium surplus of loose layer groundwater and coal sandstone groundwater were relatively more negative (Table 2), which further suggested that deep karst groundwater was affected by the evaporation effect in the process of runoff.

3.4.3 Relationship between ion concentrations and TDS

According to Figure 8A, it can be seen that the ion concentrations of Ca^{2+}, Mg^{2+} and Na^+ increased linearly with the increase of TDS, where the increase in Na^+ concentration was

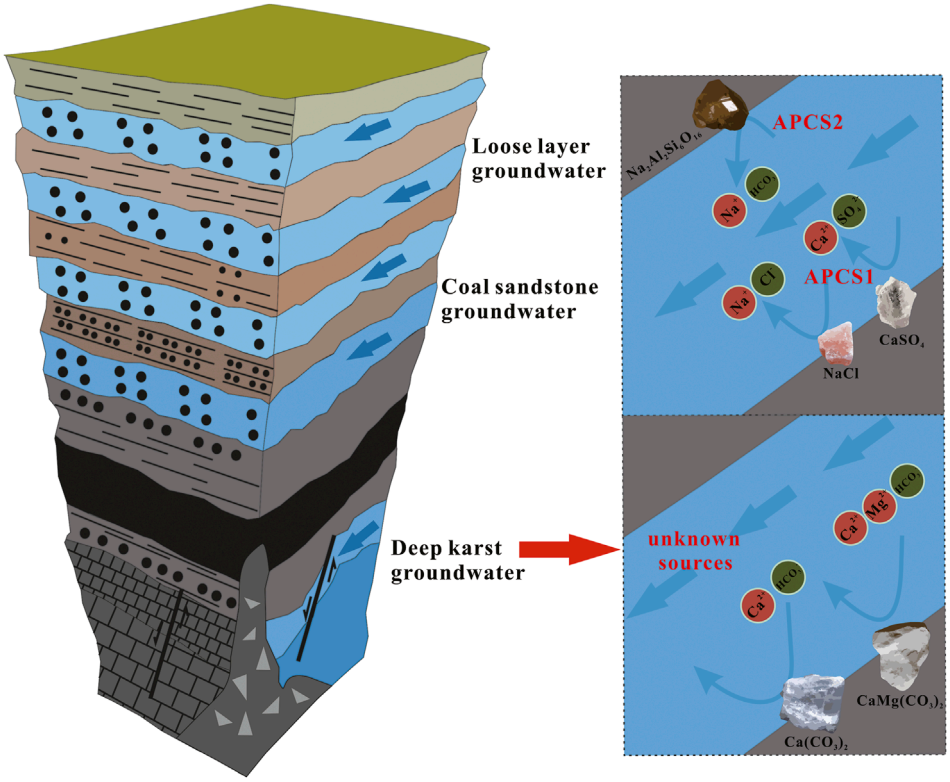

FIGURE 11
Factors influencing the hydrogeochemical evolution of deep karst groundwater.

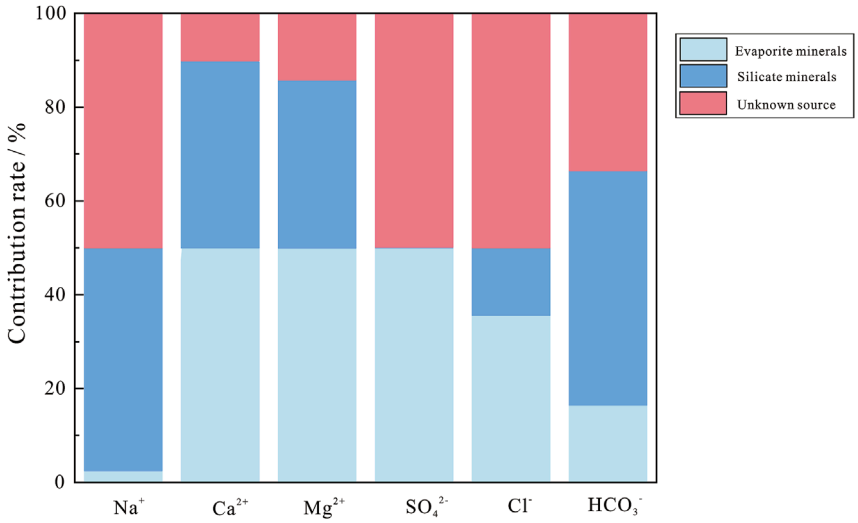

FIGURE 12
Contribution of different sources to hydrochemical indicators in karst groundwater.

slightly larger than the increase in Ca^{2+} and Mg^{2+} concentrations, which indicated that the increase of Na^{+} concentration contributes to the increase of TDS slightly more than the increase of Ca^{2+} and Mg^{2+} concentrations. According to Figure 8B, it can be seen that the ion concentrations of SO_4^{2-} and Cl^{-} also increased linearly with the increase of TDS, where the increase in SO_4^{2-} concentration was much higher than the increase in Cl^{-} concentration, while HCO_3^{-} concentration showed a linear decrease. It can be preliminary inferred that the water-rock interactions in deep karst groundwater in study area was dominated by the weathering and dissolution of minerals containing Na^{+} and SO_4^{2-} ions, i.e., the dissolution of halite and gypsum; and there was the precipitation of minerals containing HCO_3^{-} ions, i.e., the precipitation of dolomite or calcite.

3.4.4 Relationship between ion concentrations and saturation index (SI)

The mineral saturation index (SI) is an important indicator to reveal the saturation state of minerals relative to surface water or groundwater. When the saturation index of a mineral is greater than zero, it indicates that the mineral is over-saturated in the water body with a tendency to precipitate; when the saturation index of a mineral is less than zero, it indicates that the mineral is in an unsaturated state with a tendency to dissolve (Liu et al., 2023; Zou et al., 2023; Xue et al., 2024).

From Figures 9A, B, it can be seen that the concentrations of Ca^{2+}, Mg^{2+} and HCO_3^- fluctuated irregularly with the increase in the SI values of dolomite and calcite. This might be due to the fact that the SI values of calcite and dolomite were in over-saturated state with a tendency to precipitate, which in turn led to the fact that the ion concentrations of Ca^{2+}, Mg^{2+}, and HCO_3^- changed irregularly with the increase in the SI values of calcite and dolomite.

From Figure 9C, it can be seen that the ion concentrations of Ca^{2+} and SO_4^{2-} increased with the increase in the SI values of gypsum with a good exponential growth relationship. It might be due to the fact that the gypsum was always in an unsaturated state and was continuously dissolved in the karst groundwater, whereas the increase in SO_4^{2-} concentration was much greater than that in Ca^{2+} concentration, which further suggested that there might be other losses of Ca^{2+} such as precipitation of calcite and dolomite. From Figure 9D, it can be seen that as the SI values of halite increased, the concentrations of Na^+ and Cl^- increased linearly. This might be due to the fact that halite was always in an unsaturated state and was constantly dissolved in karst groundwater, and the increase in Na^+ concentration was greater than the increase in Cl^- concentration, which further suggested that there might be other sources of Na^+ such as silicate mineral dissolution and cation exchange.

3.4.5 Relationship between saturation index (SI) and TDS

As can be seen in Figure 10, the mean values of the saturation indices of dolomite, calcite, gypsum, and halite in karst groundwater were 1.3, 0.7, - 1.6, and - 5.9, respectively, and the saturation indices of dolomite and calcite were significantly higher than those of gypsum and halite. Specifically, the saturation indices of dolomite and calcite ranged from 0.33 to three and from - 0.8 to 2, respectively, indicating that calcite and dolomite were in saturated and over-saturated state in karst groundwater and tended to precipitate in the groundwater; whereas the saturation indices of gypsum and halite ranged from - 3.86 to - 0.37 and from −6.87 to −4.73, respectively, indicating that gypsum and halite were in an unsaturated state and continued to dissolve in karst groundwater. In addition, the saturation index of gypsum had the largest spatial variation among all minerals, which was mainly related to the confinement degree of the deep karst aquifer and the ionic stability of SO_4^{2-}. When the deep karst aquifer was disturbed by coal mining and changed from a closed environment to an open environment, sulphides in the adjacent coal seams would enter into deep karst groundwater, while the oxidation of sulphides was accelerated by the escape of CO_2(g) and the dissolution of O_2(g), which would result in an increase in the concentration of SO_4^{2-} in deep groundwater.

3.5 Contribution analysis of deep groundwater sources

3.5.1 Identification of impact factor

The deep groundwater environment is complex and affected by many factors, not only by natural factors such as hydrogeological conditions and geological effects, but also by anthropogenic factors such as coal mining, so how to accurately identify the influencing factors and determine the degree of influence has always been a difficult point in the study of groundwater hydrochemistry. Previous studies to identify the impact of geological effects, mainly water-rock interaction, on the hydrochemical characteristics of groundwater have focused on qualitatively determining the impact of water-rock interaction on groundwater through changes in hydrochemical components (Jin et al., 2020; Huang et al., 2022; Lu et al., 2024), but the impact extent of different water-rock interaction could not be determined (Bao et al., 2021; Liu et al., 2024; Razi et al., 2024; Zhang et al., 2024). Based on the qualitative study of the hydrochemical characteristics of karst groundwater in the study area, the factors affecting the hydrochemical components of karst groundwater were identified using principal component analysis (PCA), and a multiple linear regression (MLR) method was constructed between the predicted concentration and the actual concentration, and an APCS-MLR quantitative identification model was set up for quantitatively identifying the effects of different types of water-rock interactions on the hydrochemistry of groundwater, which could help to better understand the mechanism of groundwater genesis and provide theoretical support for sustainable use of deep groundwater.

Six indicators, including Na^+, Ca^{2+}, Mg^{2+}, Cl^-, SO_4^{2-} and HCO_3^-, which are more closely related to water-rock interactions, were selected for principal component analysis (PCA). After the data standardization, the KMO-Bartlett spherical test was performed using SPSS 21 for the correlation of the variables, and the results showed that the KMO was 0.54, and the P value of Bartlett was 0, which basically met the conditions of principal component analysis. After great orthogonal rotation of variance, two APCS with eigenvalues greater than one were extracted, with a cumulative contribution rate of 88.63% (Table 3), which basically explained most of the hydrochemistry information of deep karst groundwater in the study area.

As shown in Table 3, the contribution of APCS1 was 59.57%, and four indicators such as Ca^{2+}, Mg^{2+}, Cl^- and SO_4^{2-} had large loads, with the loads reaching 0.89, 0.91, 0.91 and 0.98, respectively, and the correlation of the three indicators such as Ca^{2+}, Mg^{2+}, and SO_4^{2-} was significant (Figure 4), indicating a consistent source. From the ion source analysis, Ca^{2+}, Mg^{2+} and SO_4^{2-} in groundwater mainly originated from the weathering and dissolution of sulphate minerals, and Cl^- mainly originated from the dissolution of halite, so APCS1 could be defined as evaporite minerals (Figure 11). The contribution of APCS2 was 29.06%, and the main loads were mainly Na^+ and HCO_3^-, with the loads reaching 0.96 and 0.7, and the correlation of Na^+ and HCO_3^- indicators was significant, indicating a consistent source. Combined with the analysis of saturation index, the carbonate minerals in karst groundwater were generally in saturated state, while silicate minerals and evaporite minerals were in an unsaturated state, so it can be deduced that both Na^+ and HCO_3^-

were the main products of the dissolution of the silicate minerals, and APCS2 could be defined as silicate minerals (Figure 11).

3.5.2 Analysis of contributions from different sources

Based on the results of the APCS-MLR receptor model analysis, the linear functional relationship between the measured and predicted results of the major ions was established, and the fitting curves were plotted. The linear fitting results showed that the R^2 values of were above 0.75 with the maximum value reaching 0.92, and the ratios of the measured values to the predicted values were generally close to 1, indicating that the analysis of the APCS-MLR receptor model were credible.

As can be seen in Figure 12, the contribution of evaporite minerals (ACPS1) to the Na^+, Ca^{2+}, Mg^{2+}, Cl^-, SO_4^{2-} and HCO_3^- were 2.47%, 50.00%, 49.97%, 35.62%, 50.02% and 16.45%, respectively, showing that weathering dissolution of evaporite minerals was the main controlling factor for Ca^{2+}, Mg^{2+}, Cl^- and SO_4^{2-} of karst groundwater. The contribution of silicate minerals (ACPS2) to Na^+, Ca^{2+}, Mg^{2+} and HCO_3^- was 47.53%, 39.86%, 35.84% and 50.01%, respectively, with a smaller contribution to other indicators, showing that weathering and dissolution of silicate minerals was the main controlling factor for Na^+ and HCO_3^- in karst groundwater. In addition, unknown sources still had high contribution to Na^+, Cl^-, SO_4^{2-} and HCO_3^- with 49.99%, 50.02%, 49.86%, and 33.54%, respectively.

Overall, the three types of factors such as evaporite minerals, silicate minerals and unknown source had the following influences on the hydrochemistry of deep karst groundwater: 59.57%, 29.06% and 11.37%, respectively. Evaporite minerals had the greatest influence on the hydrochemistry, followed by silicate minerals, and evaporite minerals and silicate minerals were the main controlling factors for the hydrochemistry of deep karst groundwater in the study area.

4 Conclusion

Mathematical statistics, graphical methods, saturation index, ion ratio and APCS-MLR receptor model were performed to investigate the hydrochemical evolution of deep karst groundwater. The main conclusions can be drawn below:

(1) The dominant cations in karst groundwater are Na^+ and Ca^{2+}, and the dominant anions are HCO_3^- and SO_4^{2-}. The hydrochemical types of the groundwater are mainly of the HCO_3.SO_4 - Na and SO_4 - Ca types.
(2) Water-rock interaction plays a controlling role on the hydrochemical components, in which the weathering dissolution of silicate minerals and evaporite minerals are the main types of water-rock interaction.
(3) In the process of recharging the deep karst groundwater by atmospheric precipitation, the water body is subjected to a certain degree of evaporation, which results in the isotopic fractionation of hydrogen and oxygen.
(4) Based on the relationship between ion concentrations, TDS and the saturation index, calcite and dolomite are always in saturated state and precipitating, and halite and gypsum are in an unsaturated state and continually dissolved.
(5) Two APCS with eigenvalues greater than 1 were extracted, where APCS1 can be defined as evaporite minerals and APCS2 can be defined as silicate minerals with a cumulative contribution of 88.63%.
(6) The hydrochemical components of deep karst groundwater mainly come from three sources, including evaporite minerals, silicate minerals and unknown sources, and the contributions to the deep groundwater are 59.57%, 29.06% and 11.37%, respectively. The weathering and dissolution of evaporite minerals and silicate minerals are the main sources of the hydrochemical components, and also the main driving factors for the groundwater evolution of deep karst groundwater.

Data availability statement

The original contributions presented in the study are included in the article/Supplementary Material, further inquiries can be directed to the corresponding authors.

Author contributions

WG: Conceptualization, Data curation, Formal Analysis, Writing–original draft. CZ: Funding acquisition, Methodology, Resources, Writing–review and editing. JM: Writing–review and editing, Investigation. YS: Writing–review and editing. HZ: Data curation, Investigation, Writing–review and editing. PX: Data curation, Investigation, Writing–review and editing. MJ: Writing–review and editing.

Funding

The author(s) declare that financial support was received for the research and/or publication of this article. This research was financially supported by National Natural Science Foundation of China (42303034), Scientific Research Projects of Colleges and Universities in Anhui Province (2022AH040210 and 2024AH051826), Key Scientific Research Project of Suzhou University (2022yzd01 and 2023yzd08), Scientific research platform open project of Suzhou University (2022ykf19) and Provincial College Students Innovation and Entrepreneurship Training Program Project (S202310379192).

Conflict of interest

The authors declare that the research was conducted in the absence of any commercial or financial relationships that could be construed as a potential conflict of interest.

Generative AI statement

The author(s) declare that no Generative AI was used in the creation of this manuscript.

Publisher's note

References

Abdelaziz, S., Gad, M. I., and El Tahan, A. H. M. H. (2020). Groundwater quality index based on PCA: wadi El-Natrun, Egypt. *J. Afr. Earth Sci.* 172, 103964. doi:10.1016/j.jafrearsci.2020.103964

Abdrashitova, R. N., and Kadyrov, M. A. (2022). Causes of variability in groundwater salinity of the lower jurassic sediments in the talinskoye oilfield of west siberia. *Sustainability* 14 (13), 7675. doi:10.3390/su14137675

Athauda, A. M. N., Abinaiyan, I., Liyanage, G. Y., Bandara, K. R., and Manage, P. M. (2023). Spatio-temporal variation of water quality in the yan oya River Basin, Sri Lanka. *Water Air Soil Poll.* 234 (3), 207. doi:10.1007/s11270-023-06151-9

Bao, Y. A., An, C., Wang, C. Y., Guo, C., and Wang, W. B. (2021). Hydrogeochemical characteristics and water-rock interactions of coalbed-produced water derived from the dafosi biogenic gas field in the southern margin of ordos basin, China. *Geofluids* 2021, 1–13. doi:10.1155/2021/5972497

Bian, J. M., Sun, W. H., Li, J. L., Li, Y. H., Ma, Y. X., and Li, Y. M. (2023). Hydrochemical formation mechanism of mineral springs in Changbai Mountain (China). *Environ. Earth Sci.* 82 (6), 145. doi:10.1007/s12665-023-10795-5

Chen, H., Wang, J. D., Zhang, F., Zhou, Y. X., Xia, C. Y., Zhang, W. L., et al. (2022). Hydrochemical characteristics and formation mechanisms of groundwater in west Zoucheng City, Shandong Province, China. *Environ. Monit. Assess.* 194 (8), 573. doi:10.1007/s10661-022-10136-2

Chen, L. W., Tian, Y., Wang, Y. X., Ou, Q. H., Peng, Z. H., Shi, X. P., et al. (2023). Water abundance evaluation model of unconsolidated confined aquifer considering sedimentary characteristics: a case study in the Su-Lin mining areas, China. *Acta. Geophys.* 71 (6), 2941–2954. doi:10.1007/s11600-023-01021-8

Chen, X., Zheng, L. G., Dong, X. L., Jiang, C. L., and Wei, X. P. (2020). Sources and mixing of sulfate contamination in the water environment of a typical coal mining city, China: evidence from stable isotope characteristics. *Environ. Geochem. Hlth.* 42 (9), 2865–2879. doi:10.1007/s10653-020-00525-2

Chen, Y. F., Chen, L. W., Peng, Z. H., Zhang, M., Hu, Y. S., Oua, Q., et al. (2023). An improved model to predict the water-inrush risk under an unconsolidated confined aquifer based on analytic hierarchy process and information value method. *Geomat. Nat. Haz. Risk* 14 (1), 2236277. doi:10.1080/19475705.2023.2236277

Fatima, S. U., Khan, M. A., Siddiqui, F., Mahmood, N., Salman, N., Alamgir, A., et al. (2022). Geospatial assessment of water quality using principal components analysis (PCA) and water quality index (WQI) in Basho Valley, Gilgit Baltistan (Northern Areas of Pakistan). *Environ. Monit. Assess.* 194 (3), 151. doi:10.1007/s10661-022-09845-5

Gu, C. C., Zhai, X. R., Wu, J. W., Li, G. P., Wang, X., Tan, P. F., et al. (2023). Structures, deformation history and dynamic background of the qianyingzi coal mine in the Huaibei coalfield, eastern China. *Front. Earth Sc* 10, 1014918. doi:10.3389/feart.2022.1014918

Huang, P., Ma, C. M., and Zhou, A. G. (2022). Assessment of groundwater sustainable development considering geo-environment stability and ecological environment: a case study in the Pearl River Delta, China. *Environ. Sci. Pollut. R.* 29 (12), 18010–18035. doi:10.1007/s11356-021-16924-6

Jiang, C. L., Jiang, C. H., Zha, J. Z., Liu, H., Liu, D., and Zheng, L. G. (2023). Water chemistry and stable isotope characteristics of subsidence lakes in coal mining areas, Eastern China. *Environ. Sci. Pollut. R.* 30 (15), 43152–43167. doi:10.1007/s11356-023-25285-1

Jin, J., Zhao, Y. P., Liu, D., Chen, Y. F., and Ding, H. J. (2020). Quantitative evaluation of the groundwater environment: a case study in Tongliao, China. *Hum. Ecol. Risk Assess.* 26 (9), 2367–2389. doi:10.1080/10807039.2020.1761245

Ju, Q. D., Hu, Y. B., Liu, Q. M., Liu, Y., and Hu, T. F. (2022). Key hydrological process of a multiple aquifer flow system in the mining area of Huaibei plain, Eastern China. *Appl. Geochem.* 140, 105270. doi:10.1016/j.apgeochem.2022.105270

Li, S. J., Su, H., Han, F. P., and Li, Z. (2023). Source identification of trace elements in groundwater combining APCS-MLR with geographical detector. *J. Hydrol.* 623, 129771. doi:10.1016/j.jhydrol.2023.129771

Li, W. Q., Wu, J. H., Zhou, C. J., and Nsabimana, A. (2021). Groundwater pollution source identification and apportionment using PMF and PCA-APCS-MLR receptor models in tongchuan city, China. *Arch. Environ. Con. Tox.* 81 (3), 397–413. doi:10.1007/s00244-021-00877-5

Liu, J., Wang, H., Jin, D. W., Xu, F., and Zhao, C. H. (2020). Hydrochemical characteristics and evolution processes of karst groundwater in Carboniferous Taiyuan formation in the Pingdingshan coalfield. *Environ. Earth Sci.* 79 (6), 151. doi:10.1007/s12665-020-8898-4

Liu, L., Wang, G. L., Li, Y. L., Wei, Z. A., Lin, W. J., Qin, X. N., et al. (2024). Hydrogeochemistry of geothermal water in Huangshadong and adjacent areas of Guangdong province: implications for water-rock interaction. *Geothermics* 122, 103084. doi:10.1016/j.geothermics.2024.103084

Liu, Z. J., Wang, X. H., Jia, S. Q., and Mao, B. Y. (2023). Eutrophication causes analysis under the influencing of anthropogenic activities in China's largest fresh water lake (Poyang Lake): evidence from hydrogeochemistry and reverse simulation methods. *J. Hydrol.* 625, 130020. doi:10.1016/j.jhydrol.2023.130020

Lu, C. Y., Wu, C., Sun, Q. Y., Wu, X., Yan, L. J., and Qin, T. (2024). Seasonal river-lake-groundwater coupling simulation and groundwater overexploitation and ecological environment assessment in the Aiding Lake Basin, NW China. *J. Hydrol.* 632, 130896. doi:10.1016/j.jhydrol.2024.130896

Lu, Z., Tao, M. X., Li, Q. G., Wu, P., Gu, S. G., Gao, W., et al. (2022). Gas geochemistry and hydrochemical analysis of CBM origin and accumulation in the Tucheng syncline in western Guizhou Province. *Geochem. J.* 56 (2), 57–73. doi:10.2343/geochemj.GJ22005

Mahanty, B., Lhamo, P., and Sahoo, N. K. (2023). Inconsistency of PCA - based water quality index - does it reflect the quality? *Sci. Total Environ.* 866, 161353. doi:10.1016/j.scitotenv.2022.161353

Mehana, M., Chen, F. X., Fahes, M., Kang, Q. J., and Viswanathan, H. (2022). Geochemical modelling of the fracturing fluid transport in shale reservoirs. *Energies* 15 (22), 8557. doi:10.3390/en15228557

Meng, F. A., Liang, X. J., Xiao, C. L., and Wang, G. (2022). Hydrochemical characteristics and identification of pollution ions of the springs in the south of Yanbian City, China. *Environ. Geochem. Hlth.* 44 (7), 2215–2233. doi:10.1007/s10653-021-01070-2

Mu, D. W., Wu, J. H., Li, X. F., Xu, F., and Yang, Y. Q. (2023). Identification of the spatiotemporal variability and pollution sources for potential pollutants of the Malian river water in northwest China using the PCA-APCS-MLR receptor model. *Expos. Health* 16 (1), 41–56. doi:10.1007/s12403-023-00537-0

Pan, Y. X., Zhang, Y. F., Wang, X. P., Zhao, Y., Zhang, Z. S., Wu, X. D., et al. (2023). Isotope variations and interrelationship characteristics of different water reservoirs during non-rainfall events in revegetation desert area, northwest China. *J. Hydrol.* 619, 129349. doi:10.1016/j.jhydrol.2023.129349

Poletaeva, V. I., Pastukhov, M. V., and Dolgikh, P. G. (2022). Trace element compositions and water quality assessment in the angara river source (baikal region, Russia). *Water* 14 (21), 3564. doi:10.3390/w14213564

Qiu, H. L., Gui, H. R., Xu, H. F., Cui, L., Li, Z. C., and Yu, H. (2023). Quantifying nitrate pollution sources of shallow groundwater and related health risks based on deterministic and Monte Carlo models: a study in Huaibei mining area, Huaibei coalfield, China. *Ecotox. Environ. Safe.* 249, 114434. doi:10.1016/j.ecoenv.2022.114434

Razi, M. H., Wilopo, W., and Putra, D. P. E. (2024). Hydrogeochemical evolution and water-rock interaction processes in the multilayer volcanic aquifer of Yogyakarta-Sleman Groundwater Basin, Indonesia. *Environ. Earth Sci.* 83 (6), 164. doi:10.1007/s12665-024-11477-6

Rizzo, P., Bucci, A., Sanangelantoni, A. M., Iacumin, P., and Celico, F. (2020). Coupled microbiological-isotopic approach for studying hydrodynamics in deep reservoirs: the case of the val d'Agri oilfield (southern Italy). *Water* 12 (5), 1483. doi:10.3390/w12051483

Sun, Y. T., Zhou, X. C., He, M., Yan, Y. C., Tian, J., Li, J. C., et al. (2023). Geochemical characteristics and water quality assessment of trace elements in geothermal springs in the Gulu-Yadong rift, Tibetan Plateau. *Geothermics* 111, 102720. doi:10.1016/j.geothermics.2023.102720

Tran, D. A., Goeppert, N., and Goldscheider, N. (2023). Use of major ion chemistry and trace and rare earth elements to characterize hydraulic relations, mixing processes and water-rock interaction in the Dong Van karst aquifer system, Northern Vietnam. *Hydrogeol. J.* 31 (7), 1735–1753. doi:10.1007/s10040-023-02689-4

Varol, M., Karakaya, G., and Alpaslan, K. (2022). Water quality assessment of the Karasu River (Turkey) using various indices, multivariate statistics and APCS-MLR model. *Chemosphere* 308 (2), 136415. doi:10.1016/j.chemosphere.2022.136415

Wang, G. T., Wu, J. W., Zhai, X. R., Zhang, H. M., and Bi, Y. S. (2022). Temporal variation of hydrogeochemical characteristics and processes of aquifers in the Liuqiao coal mine. *Energ. explor. Exploit.* 40 (5), 1382–1393. doi:10.1177/01445987221088621

Wang, H. C., Zuo, R. G., Carranza, E. J. M., and Madani, N. (2022). Modelling spatial uncertainty of geochemical anomalies using fractal and sequential indicator simulation methods. *Geochem-Explor. Env. A* 22 (4), 2022029. doi:10.1144/geochem2022-029

Warrack, J., Kang, M., and von Sperber, C. (2022). Groundwater phosphorus concentrations: global trends and links with agricultural and oil and gas activities. *Environ. Res. Lett.* 17 (1), 014014. doi:10.1088/1748-9326/ac31ef

Wu, J. Y., Wong, H. S., Zhang, H., Yin, Q., Jing, H. W., and Ma, D. (2024). Improvement of cemented rockfill by premixing low-alkalinity activator and fly ash for recycling gangue and partially replacing cement. *Cem. Concr. Comp.* 145, 105345. doi:10.1016/j.cemconcomp.2023.105345

Wu, J. Y., Yang, S., Williamson, M., Wong, H. S., Bhudia, T., Pu, H., et al. (2025). Microscopic mechanism of cellulose nanofibers modified cemented gangue backfill materials. *Adv. Compos. Hybrid. Ma* 8 (8), 177. doi:10.1007/s42114-025-01270-9

Xue, J. J., Ma, L., Qian, J. Z., and Zhao, W. D. (2024). Hydrogeochemical characteristics and evolution mechanism of groundwater in the guqiao coal mine, huainan coalfield, China. *Environ. Earth Sci.* 83 (1), 35. doi:10.1007/s12665-023-11333-z

Yu, F. R., Zhou, D. X., Li, Z. P., and Li, X. (2022). Hydrochemical characteristics and hydrogeochemical simulation research of groundwater in the guohe River Basin (henan section). *Water* 14 (9), 1461. doi:10.3390/w14091461

Zhang, H. T., Jiang, B. B., Zhang, H. Q., Li, P., Wu, M., Hao, J. W., et al. (2024). Water quality characteristics and water-rock interaction mechanisms of coal mine underground reservoirs. *Acs Omega* 9 (26), 28726–28737. doi:10.1021/acsomega.4c03073

Zhang, J., Chen, L. W., Hou, X. W., Ren, X. X., Li, J., and Chen, Y. F. (2022). Hydrogeochemical processes of carboniferous limestone groundwater in the yangzhuang coal mine, Huaibei coalfield, China. *Mine Water Environ.* 41 (2), 504–517. doi:10.1007/s10230-022-00861-y

Zhang, M., Chen, L. W., Yao, D. X., Hou, X. W., Zhang, J., Qin, H., et al. (2022). Hydrogeochemical processes and inverse modeling for a multilayer aquifer system in the yuaner coal mine, Huaibei coalfield, China. *Mine Water Environ.* 41 (3), 775–789. doi:10.1007/s10230-022-00851-0

Zou, C. J., Liu, Y. D., Pan, H. Y., Lei, Y. J., Yin, L. H., and Sun, Z. Y. (2023). Enrichment mechanism of fluoride in different aquifer systems of the Aksu area located in the Tarim Basin, Northwest China. *Appl. Geochem.* 151, 105606. doi:10.1016/j.apgeochem.2023.105606